

Differentiation of Urinary Stone and Vascular Calcifications on Non-contrast CT Images: An Initial Experience using Computer Aided Diagnosis

Hak Jong Lee,^{1,2,3,4} Kwang Gi Kim,⁵ Sung Il Hwang,^{1,2,3,4} Seung Hyup Kim,¹ Seok-Soo Byun,⁶ Sang Eun Lee,⁶ Seong Kyu Hong,⁶ Jeong Yeon Cho,¹ and Chang Gyu Seong⁷

The purpose of this study was to develop methods for the differentiation of urinary stones and vascular calcifications using computer-aided diagnosis (CAD) of non-contrast computed tomography (CT) images. From May 2003 to February 2004, 56 patients that underwent a pre-contrast CT examination and subsequently diagnosed as ureter stones were included in the study. Fifty-nine ureter stones and 53 vascular calcifications on pre-contrast CT images of the patients were evaluated. The shapes of the lesions including disperseness, convex hull depth, and lobulation count were analyzed for patients with ureter stones and vascular calcifications. In addition, the internal textures including edge density, skewness, difference histogram variation (DHV), and the gray-level co-occurrence matrix moment were also evaluated for the patients. For evaluation of the diagnostic accuracy of the shape and texture features, an artificial neural network (ANN) and receiver operating characteristics curve (ROC) analyses were performed. Of the several shape factors, disperseness showed a statistical difference between ureter stones and vascular calcifications ($p < 0.05$). For the internal texture features, skewness and DHV showed statistical differences between ureter stones and vascular calcifications ($p < 0.05$). The performance of the ANN was evaluated by examining the area under the ROC curves (AUC, A_z). The A_z value was 0.85 for the shape parameters and 0.88 for the texture parameters. In this study, several parameters regarding shape and internal texture were statistically different between ureter stones and vascular calcifications. The use of CAD would make it possible to differentiate ureter stones from vascular calcifications by a comparison of these parameters.

KEY WORDS: Ureter stone, CT, computer-aided diagnosis

INTRODUCTION

Acute flank pain is a common clinical problem. However, a diagnosis of ureterolithiasis may not be apparent based on history, a

physical examination, and clinical laboratory values.¹ For the diagnosis of urolithiasis, the gold standard is the use of intravenous urography (IVU). IVU can provide direct information about the presence, size, and location of any ureteral calculus and about renal function as well as the degree of a ureteral obstruction.¹

With the development of spiral and multidetector computed tomography (CT) scanners, several studies have shown that the use of unenhanced

¹From the Department of Radiology, Seoul National University College of Medicine, Seoul National University Hospital, Seoul, Korea.

²From the Department of Radiology, Seoul National University Bundang Hospital, Seoul, Korea.

³From the Department of Radiology, Institute of Radiation Medicine, Seoul National University Medical Research Center, Seoul, Korea.

⁴From the Department of Radiology, Clinical Research Institute, Seoul National University Hospital, Seoul, Korea.

⁵From the Biomedical Engineering Branch, Division of Basic & Applied Sciences, National Cancer Center, 111 Jungbalsan-ro, Ilsandong-gu, Gyeonggi-do 463-707, Korea.

⁶From the Department of Urology, Seoul National University College of Medicine, Seoul National University Bundang Hospital, Seoul, Korea.

⁷From the Department of Radiology, Seoul National University Boramae Hospital, Seoul, Korea.

Correspondence to: Kwang Gi Kim, Biomedical Engineering Branch, Division of Basic & Applied Sciences, National Cancer Center, 111 Jungbalsan-ro, Ilsandong-gu, Gyeonggi-do 463-707, Korea; tel: +82-31-9202241; fax: +82-31-7872242; e-mail: kimkg@ncc.re.kr

Copyright © 2009 by Society for Imaging Informatics in Medicine

Online publication 4 February 2009

doi: 10.1007/s10278-009-9181-0

helical CT is a safe, rapid, and highly accurate technique for the evaluation of patients with acute flank pain.²⁻⁶

Non-contrast CT does not require the use of intravenous contrast material with its associated cost and risk of adverse reactions, and an examination can be completed within a few minutes in most cases.¹ In addition, non-contrast CT often detects extraurinary pathology that is responsible for the patient symptoms. According to a recent report, CT is also more sensitive than IVU for detecting a calculus regardless of size, location, and chemical composition.¹ Detection of the tissue rim sign, a rim of soft tissue attenuation around the suspicious calcification is helpful in the differentiation between ureteral stones and a phlebolith.

However, there are a number of potential pitfalls in the interpretation of pre-contrast CT images. Phleboliths within the pelvis can often be seen along the normal anatomic course of the ureter and these phleboliths can mimic ureteral stones (Fig. 1).

A few studies have been reported regarding the analysis of stones from CT images. According to a report by Motley et al.,⁷ the composition of the urinary stone was analyzed by evaluation of the radiopacity measured in Hounsfield units (HU). These investigators reported that calcium stones could be distinguished from uric acid stones based on the HU values. Nakada et al.⁸ reported the differentiation between uric acid and calcium oxalate stones by the analysis of the attenuation and attenuation/size ratio. In addition, the state-of-the-art of the

current techniques for noninvasive differentiation of uric acid versus non-uric acid kidney stones using dual-energy CT was also introduced.⁹

Although many studies about the use of computer-aided diagnosis (CAD) have been reported regarding the lung, breast, or virtual colonoscopy, to the best of our knowledge, there have been no previous reports about the use of computerized analysis regarding the shape and internal texture for the differentiation of ureter stones from vascular calcifications.

The purpose of this study was to develop methods for the differentiation of urinary stones and vascular calcifications using CAD of pre-contrast CT images.

MATERIALS AND METHODS

Patients and Image Acquisition

From May 2003 to August 2003, 56 (37 male, 19 female) patients with confirmed ureter stones as determined from a pre-contrast CT examination and ureteroscopy were included in this study. The mean age of the patients was 46.7 (± 13.8) years. Our institutional review board did not require approval or patient informed consent for this retrospective review of previously obtained image data. Patient confidentiality, however, was protected.

CT images were acquired using a 16 multi-detector-row CT scanner (Mx8000 IDT, Philips



Fig 1. CT images showing a ureter stone and vascular calcification. **a** A CT image of 46-year-old woman shows a dense radiopaque lesion that was confirmed as a ureter stone. **b** A CT image of another patient shows vascular calcifications located just posterior of the dilated ureter.

Medical Systems, Best, The Netherlands). A pre-contrast scan was taken from the diaphragm to the floor of the urinary bladder with the following parameters: 120 kVp, automatic adjusted mAs, and 16×1.5-mm collimation. The image matrix size was 512×512 pixels. From the raw data obtained from the CT scanner, axial reconstruction images with a 5-mm thickness were analyzed.

Two urologists (H.J.L. and S.I.H., with 10 and 6 years experience of reading CT images of the genitourinary organs, respectively) identified ureter stones and other vascular calcifications by consensus. A ureter stone was defined as a dense radiopaque lesion in the ureter. A diagnosis of a ureter stone was confirmed by ureteroscopy or extraction of the stone. Pre-contrast CT scan images of 59 ureter stones and 53 vascular calcifications from 56 patients were analyzed. Images were displayed by use of a soft tissue window with a center of 100 HU and a width of 300 HU.

Image Analysis

The CT images were transferred in the Digital Imaging and Communications in Medicine (DICOM) format to a desktop personal computer (1-GHz Pentium processor with 512 MB of random access memory) for post-processing. For each CT image, stones and vascular calcifications were semi-

automatic segmented with the use of Otsu's algorithm. Otsu's algorithm is a nonparametric and unsupervised method of automatic threshold selection for picture segmentation. This procedure is very simple, utilizing only the zeroth-order and first-order cumulative moments of the gray-level histogram.⁷

To compare the image features of stones and vascular calcifications, various geometric parameters for shape and internal texture were adopted from previous studies. Figure 2 shows a schematic drawing of the steps for image processing. After manual selection of a region of interest (ROI) for the radiopaque lesion, histogram-based segmentation was performed. The images segmented were enlarged for evaluations. Several parameters regarding the shape and internal texture were evaluated.

To analyze the shape features, three separate measurements including "disperseness", "convex hull depth", and "lobulation count" were used. Disperseness quantifies the elongation of the lesion contour and the value is presented as the squared perimeter of a lesion boundary divided by the lesion area. Disperseness decreases if a lesion becomes circular in shape. The convex hull depth presents the degree of irregularity of a lesion. The contour of a lesion was first fitted with a convex hull. At each side of the fitted convex hull, the perpendicular distance from the side to the deepest

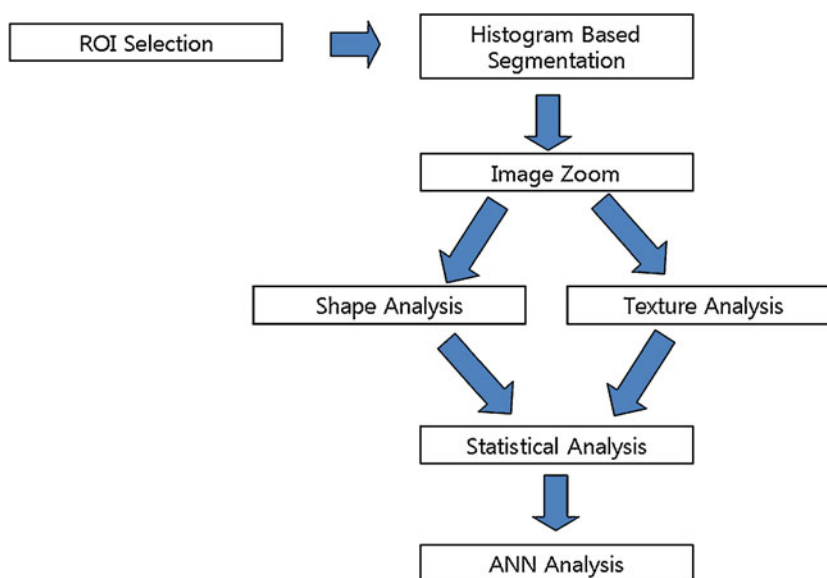


Fig 2. Schematic drawings of the steps for image processing. After region of interest (ROI) selection, histogram-based segmentation was performed. The images segmented were enlarged for evaluation. Parameters for shape and internal texture were then analyzed.

point of the contour was quantified. The distance values for all sides were summed and were normalized by the perimeter of the contour to compute the convex hull depth. The lobulation count indicate the number of lobules in the contour.¹⁰

To evaluate the internal texture of a lesion, several previously published parameters including edge density, skewness, difference histogram variation (DHV), and the gray-level co-occurrence matrix (GLCM) moment were used in the measurement of each lesion.¹¹ These parameters were computed from the gray-level values of the pixels within the lesion boundary. Edge density is defined as the mean value of edge pixels in a unit area. Skewness is defined as a measure of symmetry, or more precisely, the lack of symmetry. A distribution, or data set, is symmetric if it appears the same to the left and right of the center point. DHV is one of the texture features that can be extracted from a histogram of gray-level differences of texture. The GLCM moment is a tabulation of how often different combinations of pixel brightness values (gray levels) occur in an image. Detailed definitions of each parameter are given in [Appendix](#).

Statistical Analysis and ANN

The Student's *t* test was performed to compare the difference of parameters regarding shape and internal texture between stones and vascular calcifications. A value of $P < 0.05$ was considered as statistically significant.

For evaluation of diagnostic accuracy of the shape and texture features, a three-layered ANN with a back-propagation algorithm was used. ANN is one of the common decision support tools in current urological clinical studies. Neural networks consisted of one input layer, one hidden layer, and one output layer. All input data were normalized to a range of 0–1.0. The number of hidden units was determined by selecting the most efficient number, starting from 3. A nonlinear, sigmoid function was used as a transfer function for each of the neurons in the hidden and output layers of the networks. There was a single output node for the classification of ROI as either a vascular calcification or stone. The output value of the neural network was either 0 or 1. To obtain this output value, various thresholds were applied, which were automatically

generated using a commercially available software program (NeuroSolution; NeuroDimension, Gainesville, FL, USA) to plot the receiver operating characteristic (ROC) curve. When the output value of the ROI was greater than the threshold value, the system classified the ROI as a vascular calcification (i.e., output value of 1). Conversely, when the output value of the ROI was less than the threshold value, the system classified the ROI as stone (i.e., output value of 0). A fivefold cross-validation method was used. For each ROI, values for parameters regarding shape and texture features were calculated and were used as the input data for the ANN, respectively. The performance of the ANN was evaluated using ROC analysis for the quantitative analysis of the relevance of the features. For this method, data that were used for the training of the ANN were also used for testing. The ROCKIT algorithm (C. E. Metz, University of Chicago, IL, USA) was used to obtain the area under the ROC curve (A_z).

RESULTS

Figure 3 shows examples of histograms of a stone and of vascular calcification. The histograms show different patterns of HU distribution. Table 1 shows the mean and standard deviations of the parameters. The mean values of disperseness for stones and vascular calcifications were $5.67(\pm 4.74)$ and $3.40(\pm 1.91)$, respectively. The convex hull depth values for stones and calcifications were $-13.04(\pm 5.89)$ and $-78.33(\pm 20.44)$. Lobulation counts of stones and calcifications were $2.11(\pm 1.01)$ and $2.92(\pm 3.93)$, respectively. Among the several factors indicating shape, disperseness showed a statistical difference for vascular calcifications and ureter stones ($p < 0.05$; Fig. 4).

The mean values of the edge density of stones and calcifications were $-57.36(\pm 94.17)$ and $-116.02(\pm 142.45)$, the skewness values of stones and calcifications were $-166.65(\pm 96.11)$ and $-245.26(\pm 176.7)$, the DHV values of stones and calcifications were $3.98(\pm 0.59)$ and $3.55(\pm 0.70)$, and the mean values of the GLCM moment of stones and calcifications were $2.92(\pm 2.1)$ and $5.28(\pm 5.46)$, respectively. Among the several parameters of internal texture, skewness and the DHV showed statistical difference between the ureter stones and vascular calcifications ($p < 0.05$; Fig. 5).

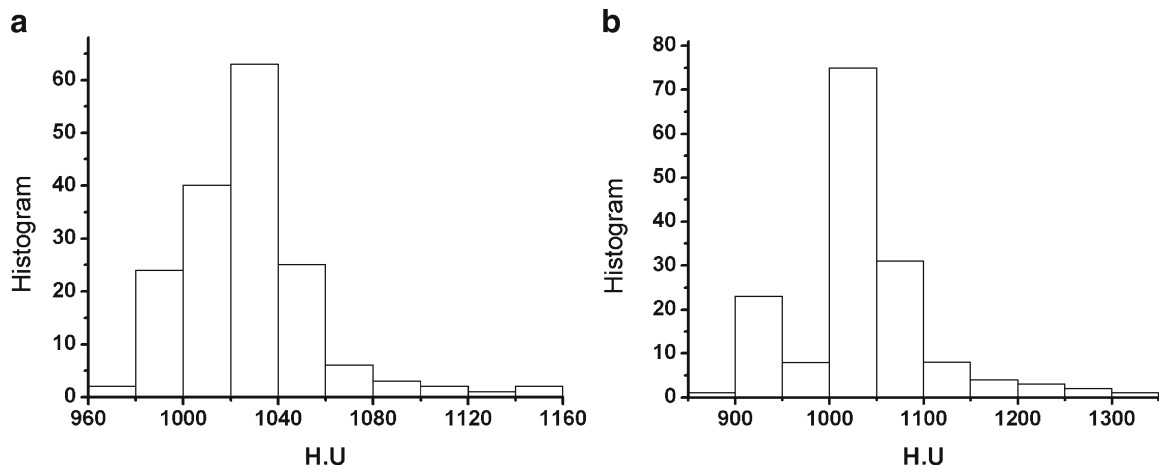


Fig 3. An example of histograms of a stone and of a vascular calcification. The histogram of a stone (a) shows relatively regular distribution of radiopacity, whereas the histogram of a vascular calcification (b) shows relatively irregular distribution of radiopacity.

Figure 6 illustrates the ROC curves of the ANN for the classification of stones and vascular calcifications. The performance of the ANN was evaluated by examination of the area under the ROC curves (A_z). The A_z value was 0.85 for the shape parameters and 0.88 for the texture parameters.

DISCUSSION

Urologists have traditionally used excretory urography (IVU) to diagnose ureteral calculi in patients. IVU can accurately determine the presence or absence of a ureteral obstruction and can provide physiological information and delineate anatomic anomalies of the collecting system and ureters.¹²

The use of IVU also has several disadvantages. It requires the use of intravenous contrast media. If the IVU shows positive findings, the study can take several hours or more to complete. IVU may fail to demonstrate the site or size of the obstruct-

ing stones.¹² In addition, IVU cannot diagnose other causes of flank pain unrelated to the urinary tract (e.g., appendicitis, diverticulitis, pancreatitis, ovarian torsion, or a ruptured aortic aneurism). The use of pre-contrast CT scans for the detection of urolithiasis has many advantages, as the procedure is safe, rapid, and accurate. A pre-contrast CT scan takes about 5 min to perform and does not expose the patient to the risk or discomfort associated with the use of intravenous contrast media. CT has a sensitivity of 0.95, a specificity of 0.98, and an accuracy of 0.97 for the diagnosis of ureteral stone disease.¹² When ureterolithiasis is present, unenhanced helical CT imaging allows precise determination of stone size and location, which is essential for patient management.¹² Furthermore, accurate localization is valuable for treatment planning^{13,14} when deciding to perform extracorporeal shock wave lithotripsy for proximal stones or ureteroscopic intervention for distal ureter stones and ureterovesical junction stones.^{13,14}

Table 1. Mean and Standard Deviation of each Parameters Regarding the Shape and Internal Texture

		Stone		Calcification		P value
		Mean	SD	Mean	SD	
Shape features	Disperseness	5.67	4.74	3.40	1.91	<0.001
	Covex hull depth	-13.04	5.89	-78.33	20.44	0.064
	Lobulation count	2.11	1.01	2.92	3.93	0.12
	Edge density	-57.36	94.17	-116.02	142.45	0.17
	Skewness	-166.65	96.11	-245.26	176.7	<0.001
Internal texture features	Difference histogram variation (DHV)	3.98	0.59	3.55	0.70	<0.001
	Gray-level co-occurrence	2.92	2.1	5.28	5.48	0.21

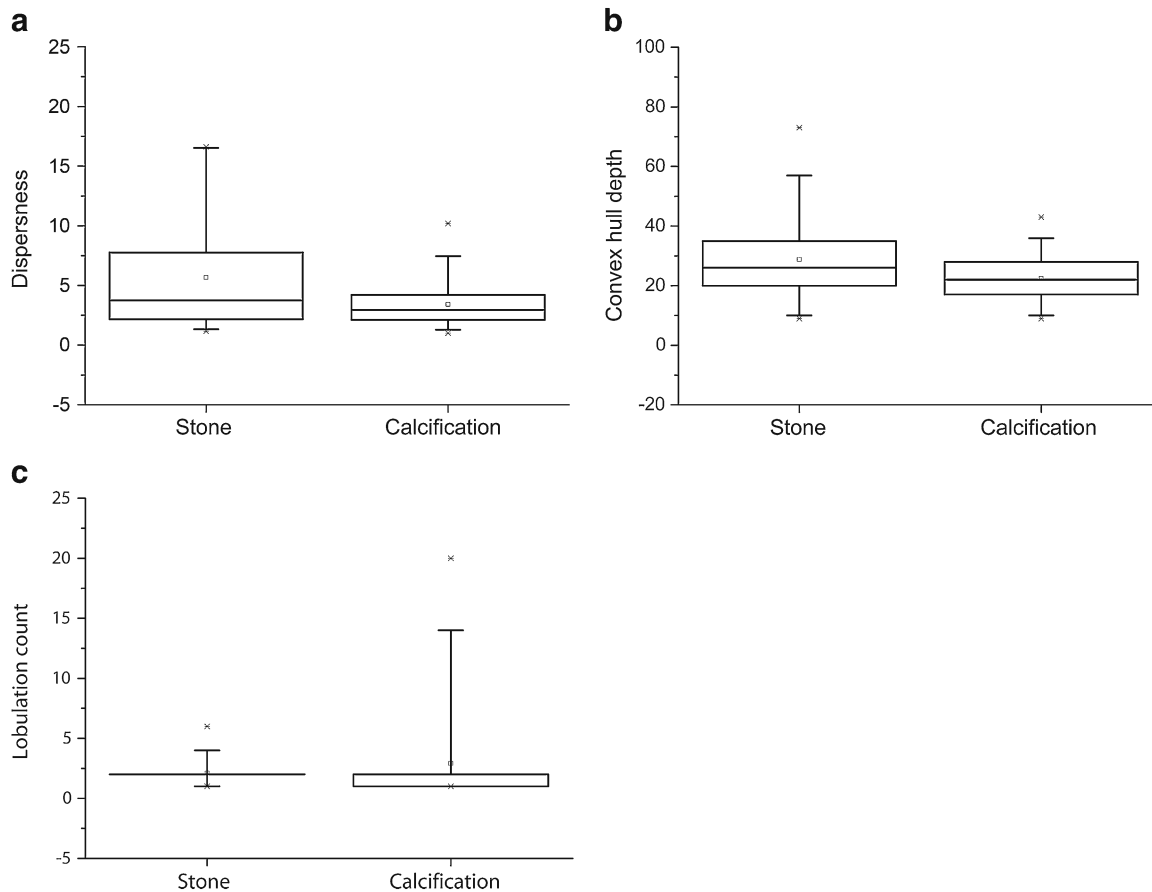


Fig 4. Graphs showing the mean and standard deviation of several parameters for shape including disperseness (a), convex hull depth (b), and lobulation count (c).

Although efforts to differentiate a urinary stone from a phlebolith have been made with the “tissue rim” or “comet tail” signs, the tissue rim sign has a disadvantage of size dependency. Smaller ureteral calculi are more likely to exhibit a tissue rim sign than larger calculi.^{15–17} According to a study by Heneghan et al., the soft tissue rim sign has been found to have a sensitivity of 77% and a specificity of 92%.¹⁸

Many studies using CAD have been reported regarding the lung, breast, and virtual colonoscopy. According to a study by Kim et al.,¹⁹ CAD identified 91% (64 of 70 lesions) and 89% (62 of 70 lesions) of malignant masses on initial and follow-up mammograms, respectively, and 100% (49 of 49 lesions) of malignant microcalcifications on both initial and follow-up mammograms. For an analysis of localized ground glass opacities, Kim et al.²⁰ reported that the area under the receiver operating characteristic curve was 0.92.

Among the several shape features, disperseness, convex hull depth, and lobulation count were evaluated. We also analyzed the internal texture by measuring the edge density, skewness, difference histogram variation, and GLCM moment. These various parameters were adopted from previous studies.^{10,20}

Our results suggest that if software for analyzing the shape and internal texture of the radiopaque lesions in the course of the ureter can be developed, the software could be used in the emergency department in situations when a radiologist was not immediately available. The software could be used as screening tool for the diagnosis of a ureter stone before radiologists interpret the CT images.

In conclusion, this study has demonstrated that several parameters regarding shape and internal texture are statistically different between ureter stones and vascular calcifications. The use of CAD

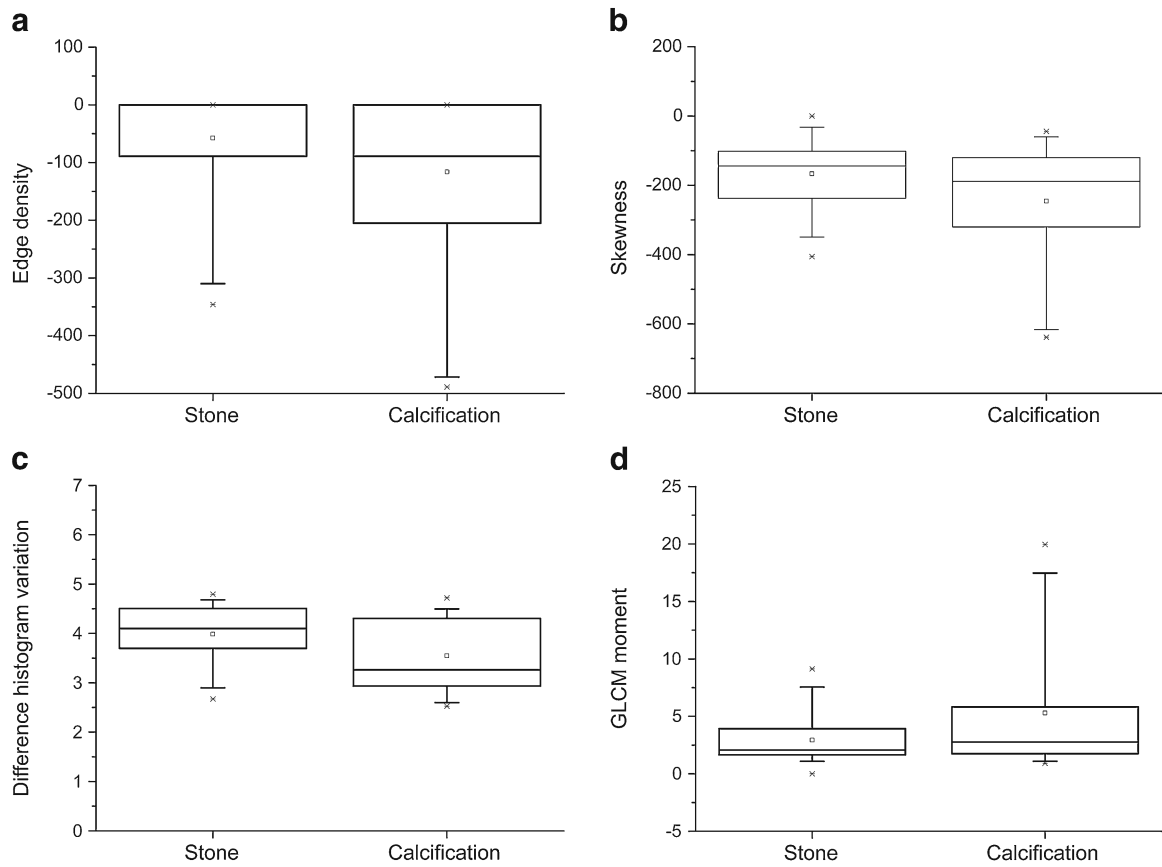


Fig 5. Graphs showing the mean and standard deviation of several parameters for internal texture including edge density (a), skewness (b), difference histogram variation (c), and the gray-level co-occurrence moment (GLCM) (d).

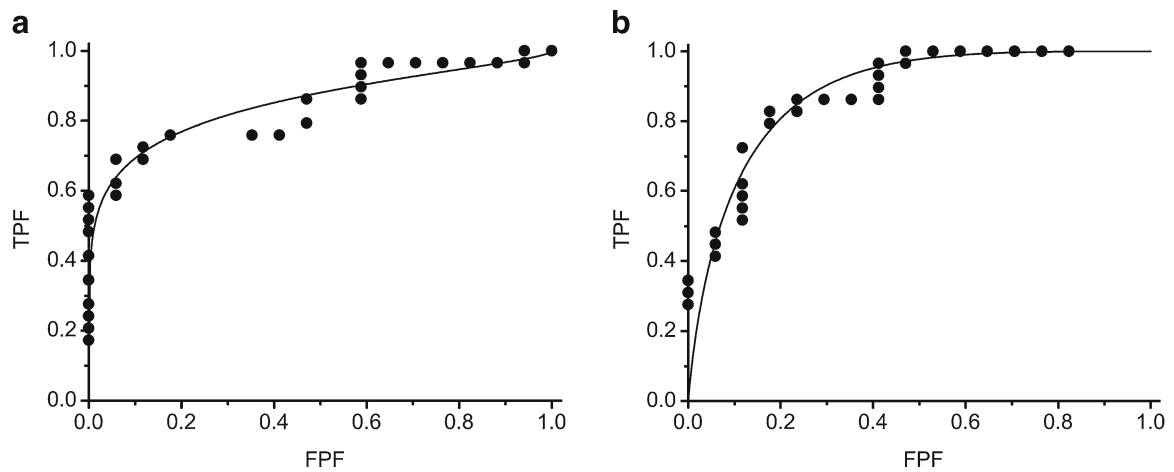


Fig 6. Graphs illustrating receiver operating characteristics (ROC) curves of the ANN for classification of stones and vascular calcifications. (a) When parameters of shape are used as the input data of the ANN, the area under curve (AUC) is 0.85. (b) When we use the parameters of internal texture are used as the input data of the ANN, the area under curve (AUC) is 0.88.

would make it possible to differentiate ureter stones from vascular calcifications by a comparison of these parameters.

ACKNOWLEDGMENT

This work was supported by the Korea Research Foundation Grant funded by the Korean Government (MOEHRD, Basic Research Promotion Fund; KRF-2005-003-E00191).

APPENDIX

1) Shape features²¹⁻²⁵

A. Disperseness

The disperseness quantifies the elongation of the lesion contour and was presented as the squared perimeter of a lesion boundary divided by the lesion area. Let p =perimeter and a =area, dispersness is $4\pi p^2/a$

B. Convex hull depth²⁴

The convex hull depth is the degree of irregularity of a lesion. The contour of a lesion was first fitted with a convex hull. At each side of the fitted convex hull, the perpendicular distance from the side to the deepest point of the contour was quantified.

C. Lobulation count^{10,26}

The lobulation count is the number of lobules in the contour.

2) Internal texture features²⁷⁻²⁹

A. Edge density

Edge density is mean value of edge pixels in unit areas. A pixel location (m,n) was declared as an edge location if its gradient $g(m,n)$ exceeded some threshold t . The location of edge points constituted an edge map $\varepsilon(m,n)$, which was defined as:

$$\varepsilon(k, l) = \begin{cases} 1, & (k, l) \in I_g \\ 0, & \text{Otherwise} \end{cases}$$

where

$$I_g \in \{(m, n); g(m, n) > t\}.$$

Given an edge map, the edge density was measured by the average number of edge pixel per unit area.¹¹

B. Skewness³⁰

Skewness is defined as a measure of symmetry, or more precisely, the lack of symmetry.

C. Difference histogram variation¹¹

Gray-level differences define the equation:

$$g(d) = |u(k, l) - u(k + d_1, l + d_2)|$$

Let $d=(d1,d2)$ be the displacement vector between two image pixels, $u(k,l)$ be the gray-level in point (k,l) , we denote $P_g(g,d)$ the histogram of the gray-level differences at the specific distance d , then we define difference histogram variation δ_d^2

$$u_d = \sum_{k=1, g=1}^N g_k p_g(g, d)$$

$$\sigma_d^2 = \sum_{k=1, g=1}^N (g_k - \mu_d^2) p_g(g, d)$$

D. Gray-level co-occurrence^{11,31}

Gray-level co-occurrence is a tabulation of how often different combinations of pixel brightness values (gray levels) occur in an image. Gray-level co-occurrence is very useful information about spatial texture organization (contrast, moment, maximum probability, homogeneity, entropy, and run-length).

Inertial of the co-occurrence matrix defined is

$$I_d = \sum_{k=1}^N \sum_{l=1}^N |k - l|^m c_{kl}$$

The coefficient is defined as $m=2$, C is co-occurrence element matrix. It attains small values in the case of coarse texture.

REFERENCES

1. Boridy IC, Nikolaidis P, Kawashima A, Sandler CM, Goldman SM: Noncontrast helical CT for ureteral stones. *World J Urol* 16:18-21, 1998
2. Smith RC, Rosenfield AT, Choe KA, et al: Acute flank pain: comparison of non-contrast-enhanced CT and intravenous urography. *Radiology* 194:789-794, 1995
3. Smith RC, Verga M, McCarthy S, Rosenfield AT: Diagnosis of acute flank pain: value of unenhanced helical CT. *AJR Am J Roentgenol* 166:97-101, 1996
4. Sommer FG, Jeffrey Jr., RB, Rubin GD, et al: Detection of ureteral calculi in patients with suspected renal colic: value of reformatted noncontrast helical CT. *AJR Am J Roentgenol* 165:509-513, 1995

5. Katz DS, Lane MJ, Sommer FG: Unenhanced helical CT of ureteral stones: incidence of associated urinary tract findings. *AJR Am J Roentgenol* 166:1319–1322, 1996
6. Smith RC, Verga M, Dalrymple N, McCarthy S, Rosenfield AT: Acute ureteral obstruction: value of secondary signs of helical unenhanced CT. *AJR Am J Roentgenol* 167:1109–1113, 1996
7. Motley G, Dalrymple N, Keesling C, Fischer J, Harmon W: Hounsfield unit density in the determination of urinary stone composition. *Urology* 58:170–173, 2001
8. Nakada SY, Hoff DG, Attai S, Heisey D, Blankenbaker D, Pozniak M: Determination of stone composition by non-contrast spiral computed tomography in the clinical setting. *Urology* 55:816–819, 2000
9. Primak A, Fletcher J, Vrtiska T, et al: Noninvasive differentiation of uric acid versus non-uric acid kidney stones using dual-energy CT. *Acad Radiol* 14:1441–1447, 2007
10. Kim KG, Cho SW, Min SJ, Kim JH, Min BG, Bae KT: Computerized scheme for assessing ultrasonographic features of breast masses. *Acad Radiol* 12:58–66, 2005
11. I P: *Digital Image Processing Algorithms and Applications*, New York: Wiley Interscience, 2000
12. Smith RC, Dalrymple NC, Neitlich J: Noncontrast helical CT in the evaluation of acute flank pain. *Abdom Imaging* 23:10–16, 1998
13. Morse RM, Resnick MI: Ureteral calculi: natural history and treatment in an era of advanced technology. *J Urol* 145:263–265, 1991
14. Dretler SP, Keating MA, Riley J: An algorithm for the management of ureteral calculi. *J Urol* 136:1190–1193, 1986
15. Dalrymple NC, Casford B, Raiken DP, Elsass KD, Pagan RA: Pearls and pitfalls in the diagnosis of ureterolithiasis with unenhanced helical CT. *Radiographics* 20:439–447, 2000
16. Guest AR, Cohan RH, Korobkin M, et al: Assessment of the clinical utility of the rim and comet-tail signs in differentiating ureteral stones from phleboliths. *AJR Am J Roentgenol* 177:1285–1291, 2001
17. Bell TV, Fenlon HM, Davison BD, Ahari HK, Hussain S: Unenhanced helical CT criteria to differentiate distal ureteral calculi from pelvic phleboliths. *Radiology* 207:363–367, 1998
18. Armato 3rd, SG, Li F, Giger ML, MacMahon H, Sone S, Doi K: Lung cancer: performance of automated lung nodule detection applied to cancers missed in a CT screening program. *Radiology* 225:685–692, 2002
19. Kim SJ, Moon WK, Cho N, Cha JH, Kim SM, Im JG: Computer-aided detection in full-field digital mammography: sensitivity and reproducibility in serial examinations. *Radiology* 246:71–80, 2008
20. Kim KG, Goo JM, Kim JH, et al: Computer-aided diagnosis of localized ground-glass opacity in the lung at CT: initial experience. *Radiology* 237:657–661, 2005
21. Chang RF, Wu WJ, Moon WK, Chen DR: Automatic ultrasound segmentation and morphology based diagnosis of solid breast tumors. *Breast Cancer Res Treat* 89:179–185, 2005
22. Keserci B, Yoshida H: Computerized detection of pulmonary nodules in chest radiographs based on morphological features and wavelet snake model. *Med Image Anal* 6:431–447, 2002
23. Li Q, Sone S, Doi K: Selective enhancement filters for nodules, vessels, and airway walls in two- and three-dimensional CT scans. *Med Phys* 30:2040–2051, 2003
24. da Fontoura Costa Jr, L: *Rmc. Shape Analysis and Classification*, Boca Raton, Florida: CRC, 2001
25. Wataru S, Kazuomi S, Yoshikazu N, Hiroaki I, Takaharu Y, Hideki Y: Three-dimensional morphological analysis of humeral heads: a study in cadavers. *Acta Orthop* 76:392–396, 2005
26. Rangayyan RM, El-Faramawy NM, Desautels JE, Alim OA: Measures of acutance and shape for classification of breast tumors. *IEEE Trans Med Imaging* 16:799–810, 1997
27. Awai K, Murao K, Ozawa A, et al: Pulmonary nodules: estimation of malignancy at thin-section helical CT—effect of computer-aided diagnosis on performance of radiologists. *Radiology* 239:276–284, 2006
28. Chen DR, Chang RF, Chen CJ, et al: Classification of breast ultrasound images using fractal feature. *Clin Imaging* 29:235–245, 2005
29. Huang SF, Chang RF, Chen DR, Moon WK: Characterization of spiculation on ultrasound lesions. *IEEE Trans Med Imaging* 23:111–121, 2004
30. Hoffman EA, Reinhardt JM, Sonka M, et al: Characterization of the interstitial lung diseases via density-based and texture-based analysis of computed tomography images of lung structure and function. *Acad Radiol* 10:1104–1118, 2003
31. Uchiyama Y, Katsuragawa S, Abe H, et al: Quantitative computerized analysis of diffuse lung disease in high-resolution computed tomography. *Med Phys* 30:2440–2454, 2003